Journal of Magnetism and Magnetic Materials 557 (2022) 169465

Contents lists available at ScienceDirect

Journal of Magnetism and Magnetic Materials

journal homepage: www.elsevier.com/locate/jmmm

Control of metamagnetic phase transition in epitaxial FeRh films by changing atomic order degree

Dezhi Zha [a,b], Baomin Wang [b,c,*], Lu Yuan [b], Yali Xie [b], Huali Yang [b], Kai Huang [b], Lan Yu [a,*], Run-Wei Li [b,d,*]

[a] School of Materials Science and Engineering, Kunming University of Science and Technology, Kunming 650093, People's Republic of China
[b] CAS Key Laboratory of Magnetic Materials and Devices and Zhejiang Province Key Laboratory of Magnetic Materials and Application Technology, Ningbo Institute of Materials Technology and Engineering, Chinese Academy of Sciences, Ningbo 315201, People's Republic of China
[c] School of Physical Science and Technology, Ningbo University, Ningbo 315211, People's Republic of China
[d] Center of Materials Science and Optoelectronics Engineering, University of Chinese Academy of Sciences, Beijing 100049, People's Republic of China

ARTICLE INFO

Keywords:
FeRh
Thermal treatment
Metamagnetic phase transition

ABSTRACT

Near-equiatomic FeRh alloys undergo a first-order metamagnetic phase transition around room temperature. Here, we show that the phase transition parameters of epitaxial FeRh films can be adjusted to a great extent through changing the growth temperature, annealing temperature, and annealing time. The influences of the surface morphology and Fe (Rh) element distribution before and after heat treatments have been analyzed. The experimental results show that the increase of annealing temperature reduces the displacement of Fe (Rh) atoms. As a result, the resistivity is reduced, the phase transition interval is narrowed, and the phase transition is shifted to high temperature. The experimental results indicate that the first-order phase transition parameters in epitaxial FeRh films can be controlled by heat treatments and are correlated with the atomic order degree of Fe (Rh).

1. Introduction

Near-equiatomic FeRh alloys exhibit metamagnetic transition from antiferromagnetic (AF) to ferromagnetic (FM) transition around room temperature [1,2], which is accompanied by changes in magnetization [3,4], entropy [5], lattice parameter [6], and resistivity [7]. Fig. 1(a) shows a typical temperature dependent magnetization curve of first-order metamagnetic transition with several important parameters: critical AF-FM transition temperature (T_t), transition temperature range ($W_{AF\text{-}FM}$), and thermal hysteresis width (W_{TH}) [8]. From the application point of view, T_t determines the operating temperature [9], while $W_{AF\text{-}FM}$ and W_{TH} are critical to the performance. For example, in the application of magnetic refrigeration technology [10], it needs a narrow W_{TH} and $W_{AF\text{-}FM}$ to obtain a greater giant magnetocaloric effect. For the successful production of controllable FM pattern in a non-magnetic background [11], the W_{TH} of the FeRh films must be wide enough to resist thermal disturbance and narrow enough for effective control. The T_t is near room temperature to facilitate the observation of the FM pattern. For the construction of some spintronic devices [12,13], a wide W_{TH} or $W_{AF\text{-}FM}$ is required to ensure a stable coexistence state with both AF and FM phases in a suitable temperature range. Therefore, the ability to control the first-order magnetic phase transition parameters (T_t, $W_{AF\text{-}FM}$ and W_{TH}) of FeRh films is particularly important for the applications.

In the past, people mainly focused on the control of T_t through different methods, such as magnetic field [14], composition adjustment [15,16], electric field induced strain [17], chemical displacement [18], and ion irradiation [19], and heat treatment [20–22]. For epitaxial FeRh films, the ion irradiation can also cause the surface layer of the film to be FM [23], while the substrate/film interface is in the AF state. Composition adjustment can produce jump-type phase transition [15]. There are few reports on the effect of heat treatment on the first-order magnetic phase transition of epitaxial FeRh films [24]. Furthermore, comparing FeRh bulk and film samples, it is found that as the annealing temperature increases, the T_t of the bulk sample decreases [25] while the film samples show the opposite properties [24]. Therefore, a systematic study of the heat treatment process is very important for the regulation of the first-order magnetic phase transition in epitaxial FeRh films. In addition, the control mechanism of heat treatment on the first-

* Corresponding authors at: CAS Key Laboratory of Magnetic Materials and Devices and Zhejiang Province Key Laboratory of Magnetic Materials and Application Technology, Ningbo Institute of Materials Technology and Engineering, Chinese Academy of Sciences, Ningbo 315201, People's Republic of China.
E-mail addresses: wangbaomin@nimte.ac.cn (B. Wang), 973819774@qq.com (L. Yu), runweili@nimte.ac.cn (R.-W. Li).

https://doi.org/10.1016/j.jmmm.2022.169465
Received 29 January 2022; Received in revised form 18 March 2022; Accepted 8 May 2022
Available online 11 May 2022

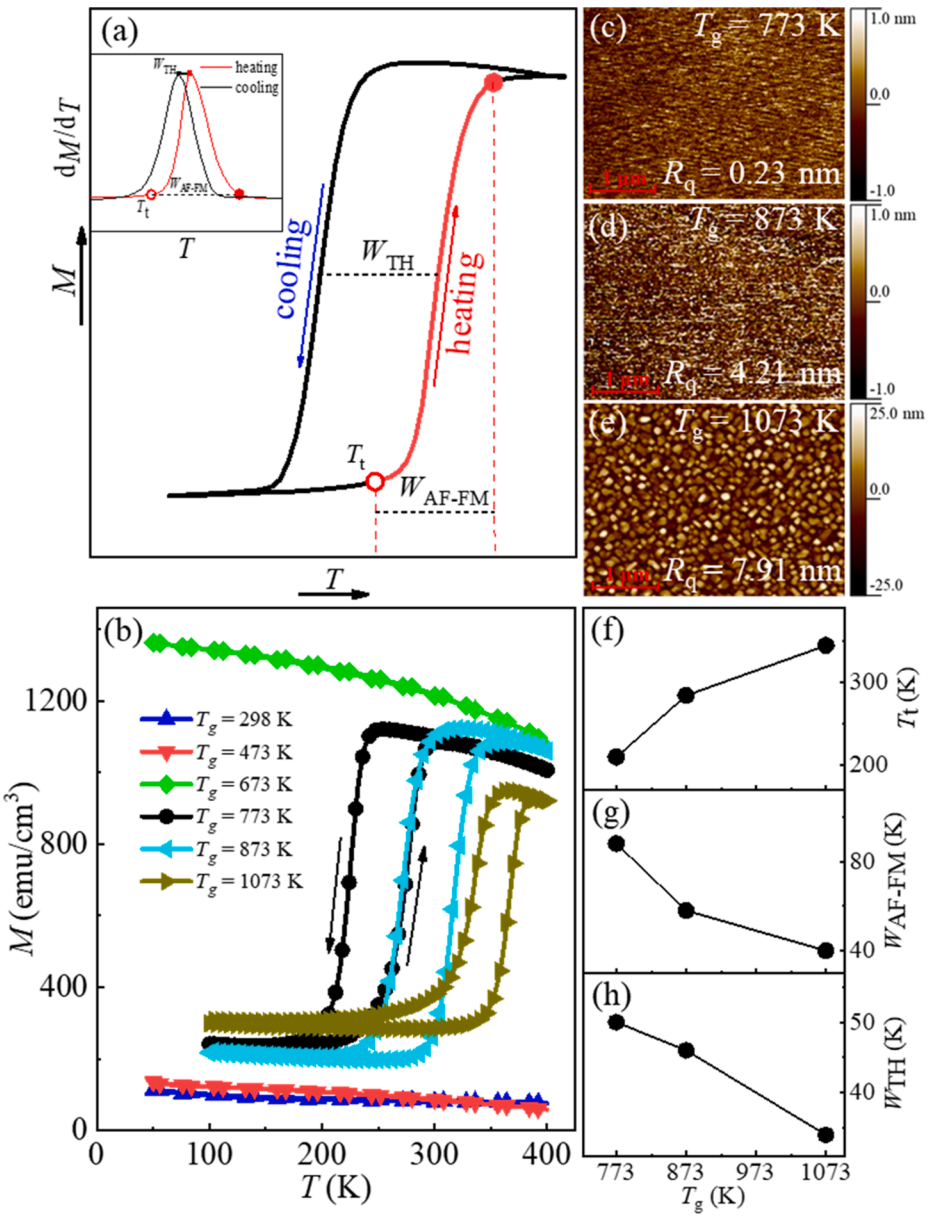

Fig. 1. (a) The temperature-dependent magnetization curve diagram is marked with first-order magnetic phase transition parameters (T_t, W_{AF-FM}, W_{TH}). The inset shows the relationship between T and dM/dT. The locations where T_t, W_{AF-FM} and W_{TH} are located are marked on the illustration. Where T_t corresponds to the critical AF-FM transition temperature of the heating curve. W_{AF-FM} is difference between T_t in the heating curve and the temperature value corresponding to just reaching saturation magnetization intensity. W_{TH} is the temperature difference between the highest points of the dM/dT curve of the heating and cooling curves. (b) Temperature-dependence magnetization curves of FeRh films for different T_g. Atomic force micrographs were taken at growth temperatures (c) T_g = 773 K, (d) T_g = 873 K and (e) T_g = 1073 K. The scanning size of atomic force micrographs is 4 × 3 μm^2. (f), (g) and (h) are the magnetic phase transition parameters T_t, W_{AF-FM} and W_{TH} with T_g, respectively.

order magnetic phase transition is still under investigation [25].

In this work, we made a systematic investigation of the effect of the thermal treatment on the first-order magnetic phase transition parameters in epitaxial FeRh films. The ways of heat treatment include growth temperature (T_g), annealing time (t_a), and annealing temperature (T_a). All of the heat treatments can regulate the first-order magnetic phase transition parameters of FeRh films. The morphology and Fe (Rh) element distribution of the films before and after heat treatments has been characterized. The experimental results indicate that the first-order magnetic phase transition parameters of the epitaxial FeRh films are correlated with the order degree of Fe (Rh) atoms.

2. Experimental

The FeRh films were prepared by an ultra-high vacuum magnetron sputtering system. Before growth, commercial (001)-oriented MgO substrates were annealed at 773 K for 1 h in a chamber with a vacuum degree of below 1 × 10^{-8} torr. The thicknesses of the FeRh films are about 30 nm, which were controlled by the growth time and were calibrated by x-ray reflectivity. In the present experiments, we used four kinds of thermal treatments: (1) FeRh films were grown at different T_g. (2) FeRh films were grown at 773 K, and then annealed at 773 K with different t_a, respectively. (3) FeRh films were grown at 773 K, and then annealed at different T_a for 1.5 h, respectively. (4) a FeRh thin film was grown at room temperature, then continuously annealed it under different T_a for 1.5 h. The thermal treatment processes of all FeRh films were completed in the chamber with a vacuum degree of below 1 × 10^{-8} torr. After the thermal treatments were completed, the films were cooled to room temperature at 0.4 K/s and then taken out from the vacuum chamber. The composition of the epitaxial FeRh thin film is close to $Fe_{51}Rh_{49}$, which is verified by the energy dispersive spectrometer.

The atomic force micrographs were collected in tapping mode using a commercial cantilever probe with a resonance frequency of about 75 kHz. The resolution is 256 × 256 pixels, the scan frequency is 1 Hz, and the scan size is 5 × 5 μm^2. The raw data processing (background subtraction, flattening and filtering) and subsequent atomic force micrograph analysis were performed using Nano Scope Analysis software.

The electrical transport of FeRh films were studied in the physical property measurement system (PPMS). The temperature-dependent electrical transport measurements were performed using the van der

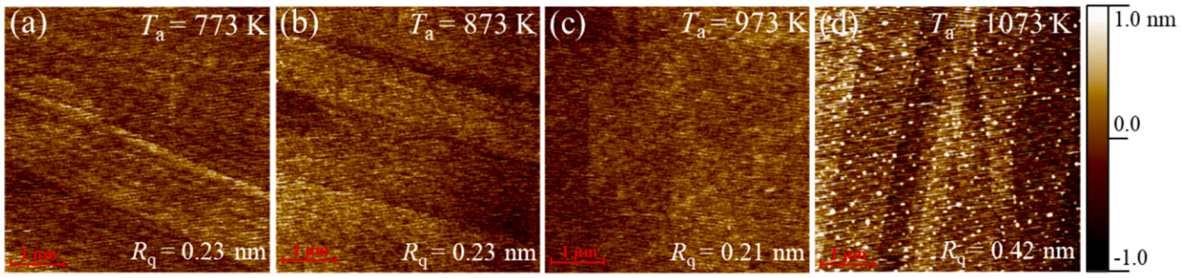

Fig. 2. Atomic force micrographs taken on FeRh films for different T_a, (a) $T_a = 773$ K, (b) $T_a = 873$ K, (c) $T_a = 973$ K, (d) $T_a = 1073$ K. The scanning size is 5×5 μm^2.

Pauw geometry with pressed Ag contacts by incrementally cycling the temperature in 2 K steps in the range of 10–400 K. The data of the magnetization in the cycle temperature of 10–400 K were collected with a superconducting quantum interferometer (SQUID-VSM) under a fixed magnetic field of 2 kOe. The temperature was swept at a typical rate of 10 K/min.

The x-ray diffraction (XRD) θ-2θ scans were performed on the D8 Bruker Advance x-ray diffractometer. During the test, a Cu target was used as the incident x-ray source, the incident wavelength was 1.5406 Å, the voltage was 40 kV, the current was 40 mA, the measured angle range was 20°-70°, and the step length of the scanning surface was 0.01°.

The cross-sectional transmission electron microscope (TEM) sample of the 30-nm-thick FeRh films was prepared from a bulk substrate, transferred to a copper grid by a manipulator and ion-milled using an Auriga focused ion-beam (FIB) instrument. Standard Ga^+ FIB operating procedures were followed (including the final polishing step, adding Pt to protect the electron beam deposition layer and reducing the thickness of the damaged part) to produce an electronically transparent FeRh/MgO thin layer. The TEM imaging described in this article was performed on a 200 kV full atomic resolution microscope (Talos F200x). A small beam flow was used to reduce the damage during TEM sample preparation. Conventional and high-resolution large-angle circular dark field (HAADF) scanning TEM (STEM) is performed on a cross-sectional transmission electron microscope slice. Mapping provides chemical element distribution analysis.

3. Results and discussions

Fig. 1(b) shows the temperature dependent magnetization curves of FeRh films growth at different T_g. The films display no first-order metamagnetic phase transition when the T_g is below 673 K, it exhibits either weak-magnetic state (grown at temperature below 473 K) or a FM state (grown at 673 K). The first-order magnetic phase transition begins to appear when the T_g is higher than 773 K. As the T_g increases, the T_t

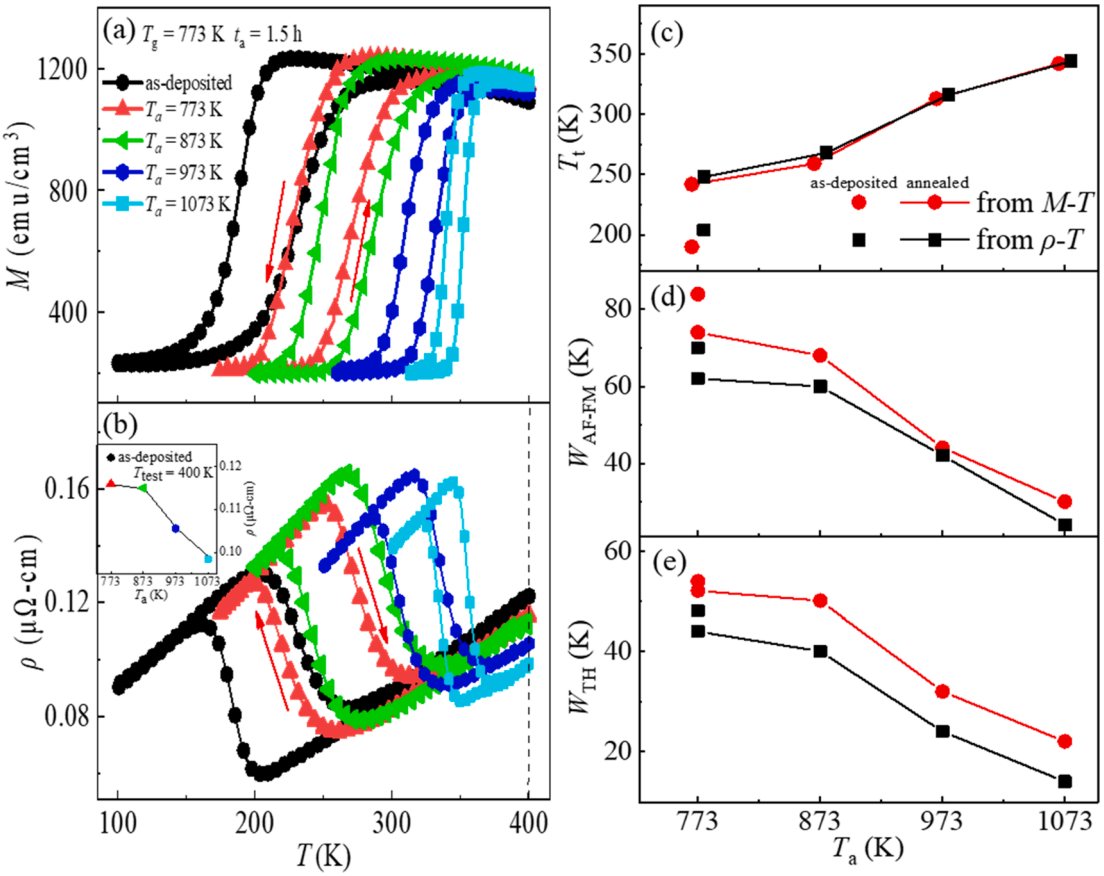

Fig. 3. (a) Temperature-dependence magnetization curves of FeRh films grown at 773 K for different T_a. (b) Temperature-dependence resistivity ρ curves of FeRh films for different T_a. The insets show relationship between ρ ($T_{test} = 400$ K) and T_a of FeRh thin films. In FeRh films, the relationship between T_a and magnetic phase transition parameters: (c) T_t, (d) W_{AF-FM} and (e) W_{TH}.

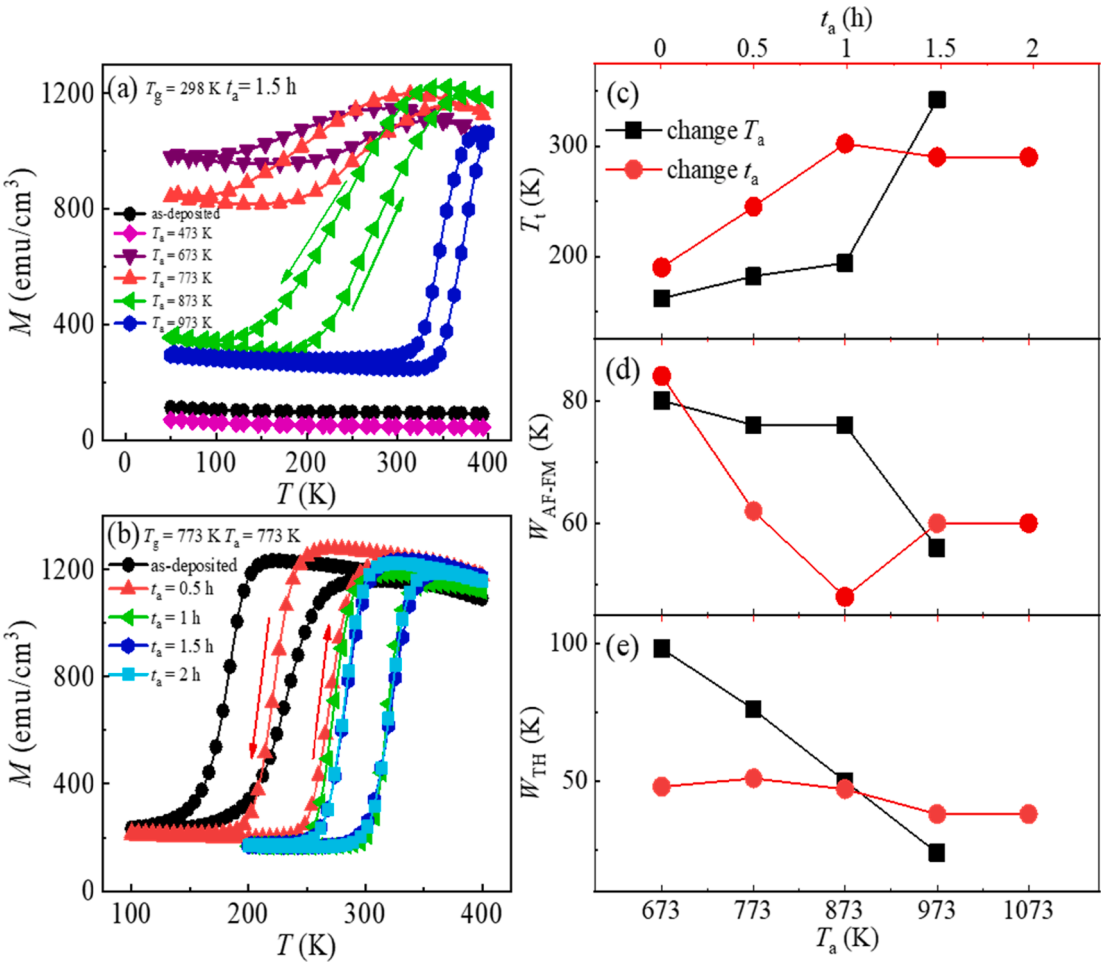

Fig. 4. (a) Temperature-dependent magnetization curves of FeRh films grown at 298 K for different T_a (same films). (b) Temperature-dependence magnetization curves of FeRh films grown at 773 K for different t_a. (c), (d) and (e) are the plots of the magnetic phase transition parameters T_t, W_{AF-FM} and W_{TH} with change T_a, respectively. Where the red curve is from the $M-T$ curve for change T_a and the black curve is from the $M-T$ curve for changing t_a.

increases significantly. It covers the common first-order metamagnetic phase transition interval of FeRh thin film. Fig. 1(c)-(e) show the roughness of the films grown at 773, 873, 1073 K, respectively. The topography results show that when the T_g of the FeRh thin film reaches 873 K, there are precipitates phase on the surface of the film [26]. The results shown in Fig. 1(f) indicate that for the thin film with T_g of 773 K, the T_t is 210 K, which can be increased to 344 K by increasing the T_g to 1073 K. Meanwhile, the W_{AF-FM} and W_{TH} decreases with increasing T_g as shown in Fig. 1(g)-(h). But the roughness of the thin film surface will also rise sharply. Considering that annealing can increase the order of FeRh B2 phase [27,28], we subsequently performed several annealing processes to control the magnetic phase transition parameters in epitaxial FeRh films.

Fig. 2(a)-(d) show the topography of the film grown at T_g = 773 K, then annealed at different T_a for 1.5 h. The surface roughness of FeRh films annealed at T_a = 773–973 K is about 0.23 nm (Fig. 2(a)-(c)). It can be seen that there are many precipitates on the FeRh thin film annealed at 1073 K (Fig. 2(d)). Both the temperature dependent magnetization and resistivity curves show that the T_a can control the magnetic phase transition parameters of FeRh films (Fig. 3(a)-(b)). In contrast to prior studies [29], it shows that the correlation between the change of magnetic phase transition parameters and the morphology is not strong. It shows that the T_a increases the T_t of the FeRh films. But when the T_a reaches 1073 K, the appearance of the precipitates increases the roughness [26].

These films all have a remanence of approximately 200 emu/cm^3 when they reach the steady state of AF as the temperature decreases. The possible origin of magnetization in the AF phase at room temperature has been proposed, such as substrate strain, changing composition, symmetry breaking, or topography of FeRh films [30–32]. Fig. 3(c)-(e) show the T_t, W_{AF-FM} and W_{TH} of magnetic phase transition parameters of FeRh films at different T_a. When T_a increases, T_t increases from 190 to 342 K in the magnetization-temperature ($M-T$) curve and from 204 to 344 K in the resistivity-temperature ($\rho-T$) curve, respectively. Meanwhile, both W_{AF-FM} and W_{TH} reduce with increasing of T_a. The magnetic phase transition parameters of FeRh thin film annealed at 1073 K is close to that in bulk FeRh [33].

Fig. 4(a) shows the $M-T$ curves of FeRh film grown at room temperature, then continuously annealed at different T_a. Lommel [34] and Ohtani [35] reported that the as-deposited and annealed FeRh films with a T_a lower than 473 K are not magnetic due to their fcc structure. In the T_a range of 673–773 K, the film exhibits higher FM, although the magnetization temperature dependence curve shows that it appears the first-order magnetic phase transition of AF-FM. However, when T_a reaches 873 K, obvious signs of AF phase have been observed at lower temperature. As the T_a further increased to 973 K, the fraction of FM phase in the film continues to decrease. The T_t, W_{AF-FM} and W_{TH} of FeRh film grown at room temperature versus T_a (Fig. 4(c)-(e)) are similar to those of film grown at 773 K (Fig. 3(c)-(e)). In addition, we have explored the influence of t_a on magnetic phase transition parameters of FeRh film (T_g = T_a = 773 K) as shown in Fig. 4(b). The T_t, W_{AF-FM} and W_{TH} are also changed with increasing of t_a (Fig. 4(c)-(e)). The results

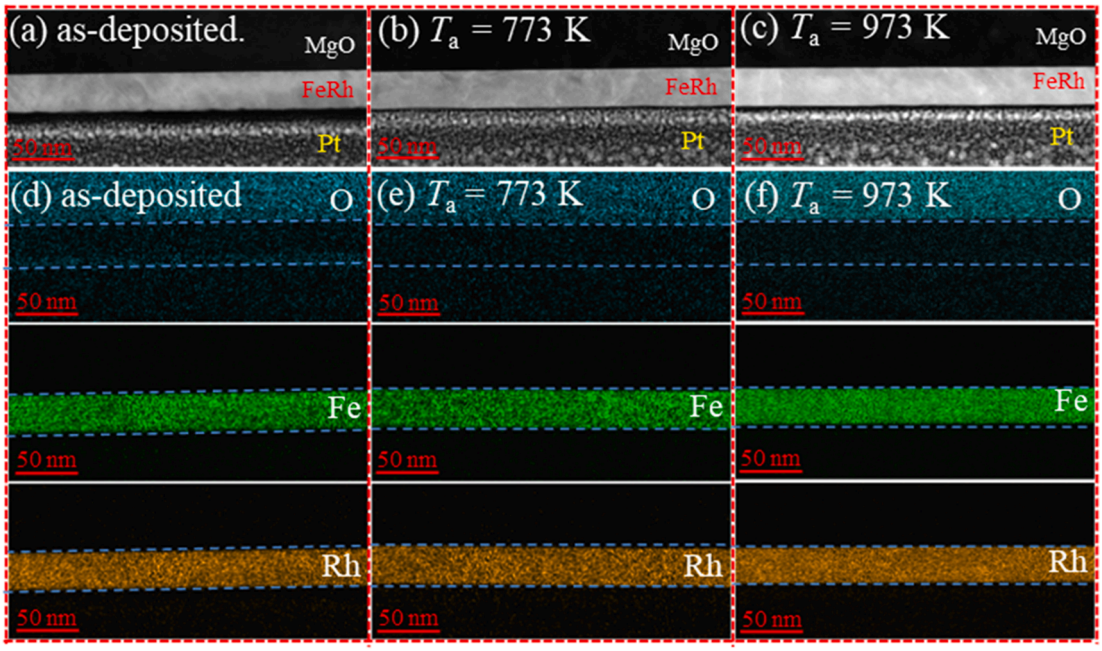

Fig. 5. (a) as-deposited, (b) $T_a = 773$ K and (c) $T_a = 973$ K HAADF-STEM images of a cross-sectional TEM lamella showing the FeRh thin film (middle of each image) grown on the MgO substrate (upper), with an average thickness of 30 nm, and protective Pt layer (lower). (d) as-deposited sample, (e) $T_a = 773$ K and (f) $T_a = 973$ K chemical composition mapping for O, Fe and Rh obtained using mapping.

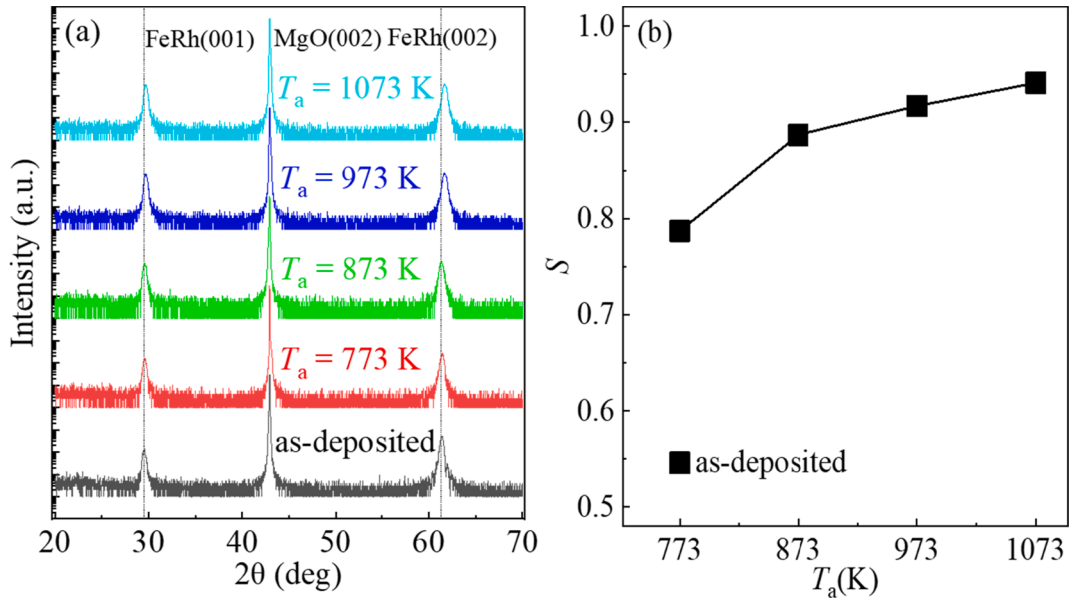

Fig. 6. (a) θ-2θ XRD diffraction patterns of FeRh films for different T_a. (b) Relationship between the order parameter S and T_a of thin films.

show that for the film with t_a no longer than 1.5 h, the magnetic phase transition parameters are greatly changed with increasing of t_a. When the t_a exceeds 1.5 h, the adjustment is weak. All these results indicate that the thermal treatments can regulate the magnetic phase transition parameters of FeRh films.

Fig. 5(a)-(c) show the images of MgO/FeRh/Pt cross sections of as-deposited, $T_a = 773$ K and $T_a = 973$ K films in HAADF-STEM mode, respectively. The FeRh films are continuous with uniform growth, and the thickness of the films are about 30 nm. Fig. 5(d)-(f) depict the element composition distribution of O, Fe and Rh of three thermal treatment films, respectively. Neither Fe nor Rh clusters are found in the micro scale. Thus, the thermal treatments may just change the arrangement order degree of Fe (Rh) atoms.

In order to investigate the atomic order degree in FeRh films, we measured the XRD of FeRh films annealed at different T_a (Fig. 6(a)). The (001) and (002) peaks were found to shift to larger angles, which indicates that the FeRh lattice shrinks. The order parameter (S) is a measure of the order quality of the epitaxial FeRh thin film, which is defined as the fraction of the Fe (Rh) atoms occupying the ideal position of the crystal lattice in the B2-FeRh crystal structure of the order condition. According to the mirror XRD scan, S can be determined as $S = ([I_{(001)}/I_{(002)}]/[I^*_{(001)}/I^*_{(002)}])^{1/2}$, where $I_{(001)}$ and $I_{(002)}$ are the integrated intensities of the superlattice Bragg peak and the basic Bragg peak respectively. $I^*_{(001)}$ and $I^*_{(002)}$ refer to the theoretical intensities calculated for each sample [36]. As shown in Fig. 6(b), the order parameter S of FeRh films rises from 0.54 in the as-deposited to 0.92

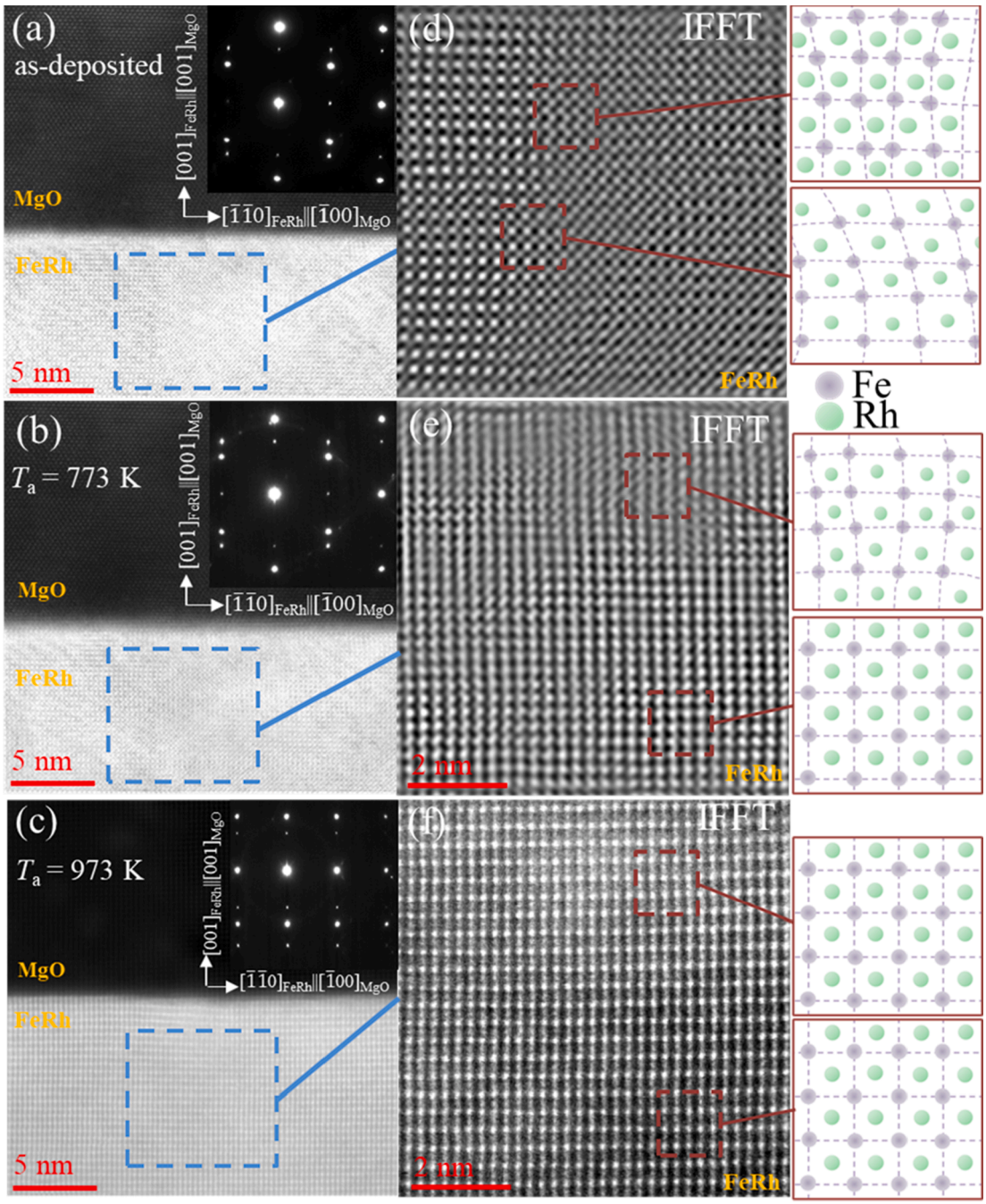

Fig. 7. (a) as-deposited, (b) T_a = 773 K and (c) T_a = 973 K HAADF-STEM images of a cross-sectional atomic scale resolution showing the FeRh films (upper) grown on the MgO (001) substrate (lower). The inset shows the a corresponding SAED pattern. (d), (e) and (f) the a corresponding IFFT pattern. The image on the right corresponds to the partial enlarged schematic diagram of IFFT.

when annealed at 973 K. The change rate of order parameter S is about 70%. This result indicates that the atomic order degree of the FeRh thin film is positively correlated with the T_a. This is consistent with the resistivity of thin films annealed at different T_a. As shown in the inset of Fig. 3(b), at 400 K, as the T_a increases, the resistivity of thin films decreases with increasing T_a. In an intact crystal, electrons basically move in a uniform electric field, while in a defective crystal, the periodicity of the lattice in the defect area is destroyed and the electric field changes sharply, which strongly scatters the electrons, resulting in the increase of resistivity in a crystal [37]. Therefore, the decrease of resistivity with the increase of T_a is due to the tendency of FeRh crystal structure to be ordered [38].

To further illustrate that the T_a increases the atomic order of FeRh films, TEM observations were carried out on samples prepared by FIB. Fig. 7(a)-(c) show the atomic images of as-deposited, 773 K and 973 K annealed films, respectively. It shows that FeRh films grows epitaxially on MgO substrate, although there are some defects. The inset of each figure shows the corresponding selected area electron diffraction (SAED) pattern, indicating that the film is a completely dense, epitaxial FeRh layer. It has a B2-ClCs structure, and the film lattice has a 45° in-plane rotation relative to the MgO (001) substrate below: $(001)_{FeRh}||(001)_{MgO}$ and $[1\,1\,0]_{FeRh}||[1\,0\,0]_{MgO}$ [11]. Fig. 7 (d)-(f) corresponds to inverse fast Fourier transform (IFFT) patterns, showing the projection of the Fe (Rh) atomic column of the corresponding film. The picture on the right is an enlarged schematic diagram of the local area in the corresponding IFFT picture. It shows that there are a large number of atomic

displacements in the as-deposited FeRh film. The atomic displacements in the FeRh film annealed at 773 K are significantly reduced, and almost no atomic displacements are seen in the film annealed at 973 K. Therefore, the increase of T_a can decrease the displacement of Fe (Rh) atoms in the film to certain extent, then reduces the compression and expansion of the lattice, which may enhance the exchange coupling force of Fe atoms in AF state [39]. As a result, T_a improves the stability of the FeRh film in the AF state, thereby increasing the T_t of the film. In the meanwhile, both $W_{AF\text{-}FM}$ and W_{TH} become narrower, this could be explained by the fact that the increase of T_a causes most of the atoms in the film to be ordered and the degree of order is close [40,41], which results in the lattice having similar transition temperatures.

4. Conclusions

In summary, by adjusting the T_g of FeRh to obtain a thin film epitaxially grown in the direction of MgO (0 0 1), with AF to FM first-order magnetic phase transition, but when the T_g reaches 873 K or more, precipitated phases will appear. We have shown that for FeRh films grown at 773 K, the T_a can increase the AF to FM initial phase transition point from 190 to 342 K. Meanwhile, both $W_{AF\text{-}FM}$ and W_{TH} are reduced. When the T_a reaches 1073 K, precipitated phases will also appear. It is worth noting that the experimental results show that the magnetic phase transition parameters changed by annealed are not strongly related to the surface morphology and element distribution of the films. As the T_a of the FeRh films increases, the perfection of the crystal structure increases, and the atomic order parameter S varies monotonously between 0.54 and 0.92. In addition, the results prove that annealed is to control the first-order magnetic phase transition by reducing the atomic displacement of thin film. Finally, we want to emphasize that the first-order magnetic phase transition can be controlled by multiple thermal treatments in the same FeRh film. In addition, the first-order magnetic phase transition parameters of FeRh films can be controlled by heat treatments in a wider range, which is essential for the development of several existing and proposed technologies.

CRediT authorship contribution statement

Dezhi Zha: Investigation, Formal analysis, Writing – original draft. **Baomin Wang:** Conceptualization, Writing – review & editing, Supervision, Funding acquisition. **Lu Yuan:** Investigation. **Yali Xie:** Formal analysis. **Huali Yang:** Formal analysis. **Kai Huang:** Investigation. **Lan Yu:** Supervision, Funding acquisition. **Run-Wei Li:** Supervision, Funding acquisition.

Declaration of Competing Interest

The authors declare that they have no known competing financial interests or personal relationships that could have appeared to influence the work reported in this paper.

Acknowledgements

This work was supported by the National Natural Science Foundation of China (51871232, 51871233, 51931011), K. C. Wong Education Foundation (GJTD-2020-11).

References

[1] M. Fallot, Propiétés magnétiques des alliages du fer avec le rhodium, C. R. Acad. Sci. 205 (1937) 558–560.
[2] M. Fallot, R. Hocart, Sur l'apparition du ferromagnétisme par élévation de température dans des alliages de fer et de rhodium, Rev. Sci. 77 (1939) 498–501.
[3] L. Muldawer, F. deBergevin, Antiferromagnetic-ferromagnetic transformation in FeRh, J. Chem. Phys. 35 (5) (1961) 1904–1905, https://doi.org/10.1063/1.1732175.
[4] C.P. Bean, D.S. Rodbell, Magnetic disorder as a first-order phase transformation, Phys. Rev. 126 (1) (1962) 104–115.
[5] J.S. Kouvel, C.C. Hartelius, Anomalous magnetic moments and transformations in the ordered alloy FeRh, J. Appl. Phys. 33 (3) (1962) 1343–1344, https://doi.org/10.1063/1.1728721.
[6] Q.J. Yap, J.J. Qiu, P. Luo, J.F. Ying, G.C. Han, D.E. Laughlin, J.-G. Zhu, T. Kanbe, T. Shige, Phase ordering and its effect on magnetic and structural properties of FeRh ultrathin films, J. Appl. Phys. 116 (4) (2014) 043902, https://doi.org/10.1063/1.4890032.
[7] P.A. Algarabel, M.R. Ibarra, C. Marquina, A. del Moral, J. Galibert, M. Iqbal, S. Askenazy, Giant room-temperature magnetoresistance in the FeRh alloy, Appl. Phys. Lett. 66 (22) (1995) 3061–3063, https://doi.org/10.1063/1.114278.
[8] S. Maat, J.-U. Thiele, E.E. Fullerton, Temperature and field hysteresis of the antiferromagnetic-to-ferromagnetic phase transition in epitaxial FeRh films, Phys. Rev. B 72 (21) (2005), https://doi.org/10.1103/PhysRevB.72.214432.
[9] J.-U. Thiele, S. Maat, E.E. Fullerton, FeRh/FePt exchange spring films for thermally assisted magnetic recording media, Appl. Phys. Lett. 82 (17) (2003) 2859–2861, https://doi.org/10.1063/1.1571232.
[10] Y. Liu, L.C. Phillips, R. Mattana, M. Bibes, A. Barthelemy, B. Dkhil, Large reversible caloric effect in FeRh thin films via a dual-stimulus multicaloric cycle, Nat. Commun. 7 (2016) 11614, https://doi.org/10.1038/ncomms11614.
[11] A.B. Mei, I. Gray, Y. Tang, J. Schubert, D. Werder, J. Bartell, D.C. Ralph, G. D. Fuchs, D.G. Schlom, Local photothermal control of phase transitions for on-demand room-temperature rewritable magnetic patterning, Adv. Mater. 32 (22) (2020) 2001080, https://doi.org/10.1002/adma.v32.2210.1002/adma.202001080.
[12] Y. Wang, M.M. Decker, T.N.G. Meier, X. Chen, C. Song, T. Grunbaum, W. Zhao, J. Zhang, L. Chen, C.H. Back, Spin pumping during the antiferromagnetic–ferromagnetic phase transition of iron–rhodium, Nat. Commun. 11 (2020) 275, https://doi.org/10.1038/s41467-019-14061-w.
[13] Y.-H. Zhang, T.-W. Weng, T.-C. Chuang, D. Qu, S.-Y. Huang, Demonstration of spin current switch across ferro-antiferromagnetic transition, Adv. Quantum Technol. 3 (10) (2020) 2000059, https://doi.org/10.1002/qute.v3.1010.1002/qute.202000059.
[14] J.S. Kouvel, Unusual nature of the abrupt magnetic transition in FeRh and its pseudobinary variants, J. Appl. Phys. 37 (3) (1966) 1257–1258, https://doi.org/10.1063/1.1708424.
[15] M. Jiang, X.Z. Chen, X.J. Zhou, Y.Y. Wang, F. Pan, C. Song, Influence of film composition on the transition temperature of FeRh films, J. Cryst. Growth. 438 (2016) 19–24, https://doi.org/10.1016/j.jcrysgro.2015.12.035.
[16] A.B. Mei, Y. Tang, J.L. Grab, J. Schubert, D.C. Ralph, D.G. Schlom, Structural, magnetic, and transport properties of $Fe_{1-x}Rh_x$/MgO (001) films grown by molecular-beam epitaxy, Appl. Phys. Lett. 113 (8) (2018) 082403, https://doi.org/10.1063/1.5048303.
[17] A.A. Amirov, I.A. Baraban, A.A. Grachev, A.P. Kamantsev, V.V. Rodionov, D. M. Yusupov, V.V. Rodionova, A.V. Sadovnikov, Voltage-induced strain to control the magnetization of bi FeRh/PZT and tri PZT/FeRh/PZT layered magnetoelectric composites, AIP Adv. 10 (2) (2020) 025124, https://doi.org/10.1063/1.5130026.
[18] R. Barua, F. Jiménez-Villacorta, L.H. Lewis, Towards tailoring the magnetocaloric response in FeRh-based ternary compounds, Journal of Applied Physics 115 (17) (2014) 17A903, https://doi.org/10.1063/1.4854975.
[19] S.P. Bennett, S.W. LaGasse, M. Currie, O.V.T. Erve, J.C. Prestigiacomo, C.D. Cress, S.B. Qadri, N^+ irradiation and substrate-induced variability in the metamagnetic phase transition of FeRh films, Coatings. 11 (2021) 661, https://doi.org/10.3390/coatings11060661.
[20] S. Inoue, N. N. Phuoc, J. W. Cao, N. T. Nam, T. Suzuki, Structural and magneto-optical properties of FeRh thin films, J. Appl. Phys. 103 (2008) 07B312, https://doi.org/ 10.1063/1.2834446.
[21] W. Lu, P. Huang, K. Li, B. Yan, Effect of substrate temperature on the crystallographic structure and first-order magnetic phase transition of FeRh thin films, J. Mater. Res. 28 (8) (2013) 1042–1046, https://doi.org/10.1557/jmr.2013.61.
[22] A. Iwase, K. Yoneda, R. Ishigami, T. Matsui, Restoration of ion beam irradiation induced metastable magnetic states and lattice structures of FeRh thin films by heat treatments at elevated temperatures, J. Magn. Magn. Mater. 515 (2020) 167286, https://doi.org/10.1016/j.jmmm.2020.167286.
[23] C.D. Cress, D. Wickramaratne, M.R. Rosenberger, Z. Hennighausen, P.G. Callahan, S.W. LaGasse, N. Bernstein, O.M. van 't Erve, B.T. Jonker, S.B. Qadri, J. C. Prestigiacomo, M. Currie, I.I. Mazin, S.P. Bennett, Direct-write of nanoscale domains with tunable metamagnetic order in FeRh thin films, ACS Appl, Mater. Interfaces. 13 (1) (2021) 836–847, https://doi.org/10.1021/acsami.0c1356510.1021/acsami.0c13565.s001.
[24] J. Cao, N.T. Nam, S. Inoue, H.Y.Y. Ko, N.N. Phuoc, T. Suzuki, Magnetization behaviors for FeRh single crystal thin films, J. Appl. Phys. 103 (7) (2008) 07F501, https://doi.org/10.1063/1.2828812.
[25] A. Chirkova, F. Bittner, K. Nenkov, N.V. Baranov, L. Schultz, K. Nielsch, T. G. Woodcock, The effect of the microstructure on the antiferromagnetic to ferromagnetic transition in FeRh alloys, Acta Mater. 131 (2017) 31–38, https://doi.org/10.1016/j.actamat.2017.04.005.
[26] M. Takahashi, R. Oshima, Annealing effect on phase transition of equiatomic FeRh alloy, Mater Trans. 36 (6) (1995) 735–742, https://doi.org/10.2320/matertrans1989.36.735.
[27] J. Ehrler, B. Sanyal, J. Grenzer, S. Zhou, R. Böttger, B. Eggert, H. Wende, J. Lindner, J. Fassbender, C. Leyens, K. Potzger, R. Bali, Magneto-structural correlations in a systematically disordered B2 lattice, New J. Phys. 22 (7) (2020) 073004, https://doi.org/10.1088/1367-2630/ab944a.

[28] Y.L. Xie, Q.F. Zhan, T. Shang, H.L. Yang, B.M. Wang, J. Tang, R.W. Li, Preparation and magnetic properties of wrinkled FeRh flexible films, AIP Adv. 7 (2017), 056314, https://doi.org/10.1063/1.5128017.
[29] J.L. Warren, C.W. Barton, C. Bull, T. Thomson, Topography dependence of the metamagnetic phase transition in FeRh thin films, Sci. Rep. 10 (2020) 4030, https://doi.org/10.1038/s41598-020-60767-z.
[30] C. Gatel, B. Warot-Fonrose, N. Biziere, L.A. Rodríguez, D. Reyes, R. Cours, M. Castiella, M.J. Casanove, Inhomogeneous spatial distribution of the magnetic transition in an iron-rhodium thin film, Nat Commun 8 (1) (2017), https://doi.org/10.1038/ncomms15703.
[31] J. W. Kim, P. J. Ryan, Y. Ding, L. H. Lewis, M. Ali, C. J. Kinane, B. J. Hickey,.
[32] C. H. Marrows, and D. A. Arena, Surface influenced magnetostructural transition in FeRh films, Appl. Phys. Lett. 95 (2009) 222515, https://doi.org/ 10.1063/1.3265921.
[33] W. Griggs, B. Eggert, M.O. Liedke, M. Butterling, A. Wagner, U. Kentsch, E. Hirschmann, M. Grimes, A.J. Caruana, C. Kinane, H. Wende, R. Bali, T. Thomson, Depth selective magnetic phase coexistence in FeRh thin films, APL Mater. 8 (12) (2020) 121103, https://doi.org/10.1063/5.0032130.
[34] V.I. Zverev, R.R. Gimaev, T. Miyanaga, A.A. Vaulin, A.F. Gubkin, B.B. Kovalev, A. M. dos Santos, E. Lovell, L.F. Cohen, N.A. Zarkevich, Peculiarities of the phase transformation dynamics in bulk FeRh based alloys from magnetic and structural measurements, J. Magn. Magn. Mater. 522 (2021) 167560, https://doi.org/10.1016/j.jmmm.2020.167560.
[35] J.M. Lommel, J.S. Kouvel, Effects of mechanical and thermal treatment on the structure and magnetic transitions in FeRh, J. Appl. Phys. 38 (3) (1967) 1263–1264, https://doi.org/10.1063/1.1709570.
[36] Y. Ohtani, I. Hatakeyama, Antiferro-ferromagnetic transition and microstructural properties in a sputter deposited FeRh thin film system, J. Appl. Phys. 74 (5) (1993) 3328–3332, https://doi.org/10.1063/1.354557.
[37] E. Yang, D.E. Laughlin, J.G. Zhu, Correction of order parameter calculations for FePt perpendicular thin films, IEEE Trans. Magn. 48 (2012) 7–12. http://ieeexplore.ieee.org.
[38] K.L. Chopra, L.C. Bobb, M.H. Francombe, Electrical resistivity of thin single-crystal gold films, J. Appl. Phys. 34 (6) (1963) 1699–1702, https://doi.org/10.1063/1.1702662.
[39] B. Eggert, A. Schmeink, J. Lill, M.O. Liedke, U. Kentsch, M. Butterling, A. Wagner, S. Pascarelli, K. Potzger, J. Lindner, T. Thomson, J. Fassbender, K. Ollefs, W. Keune, R. Bali, H. Wende, Magnetic response of FeRh to static and dynamic disorder, RSC Adv. 10 (24) (2020) 14386–14395, https://doi.org/10.1039/D0RA01410A.
[40] A. Ceballos, Z. Chen, O. Schneider, C. Bordel, L.-W. Wang, F. Hellman, Effect of strain and thickness on the transition temperature of epitaxial FeRh thin-films, Appl. Phys. Lett. 111 (17) (2017) 172401, https://doi.org/10.1063/1.4997901.
[41] E. La Torre, A. Smekhova, C. Schmitz-Antoniak, K. Ollefs, B. Eggert, B. Cöster, W. Dirk, W. Fabrice, R. Andrei, L. Jürgen, B. Rantej, B. Rudra, S. Biplab, H. Wende, Local probe of irradiation-induced structural changes and orbital magnetism in $Fe_{60}Al_{40}$ thin films via an order-disorder phase transition, Phys. Rev. B. 98 (2018), 024101, https://doi.org/10.1103/PhysRevB.98.024101.